OPEN ACCESS

Chemical Biology ARTICLE

The Innovation Drug Discovery

Target identification of celastrol based on PROTAC technology and its antitumor mechanism in MDA-MB-231 cells

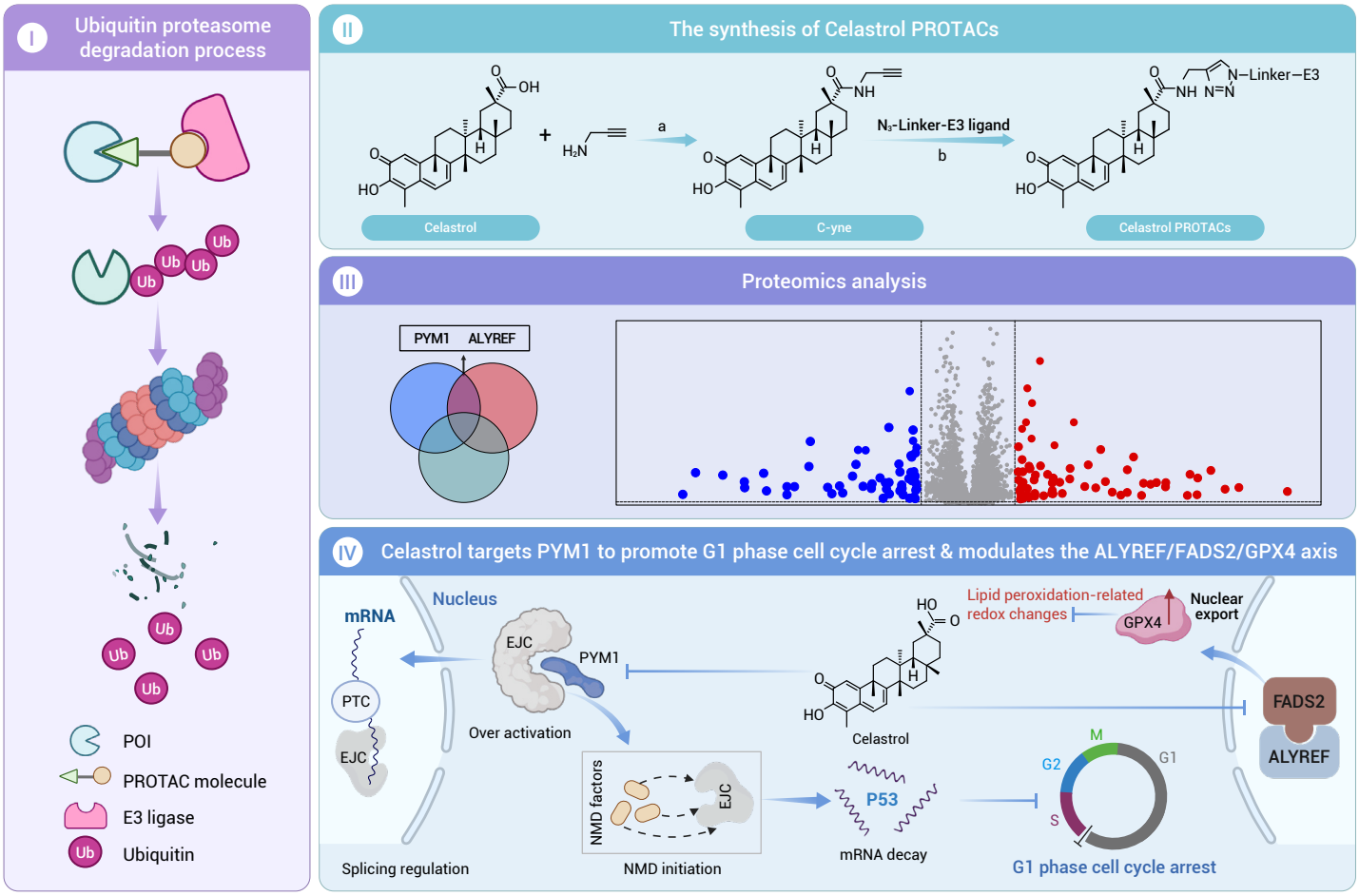
Man Zhu,[1,3] Haoze Song,[1,3] Yang Liu,[1,2,3] Kuiru Sa,[1] Hongbo Chen,[1] Yueying Yang,[1] Dejuan Sun,[1,*] Hua Li,[2,*] and Lixia Chen[1,*]

*Correspondence: sywysdj@163.com (D.S.); lihua@fjtcm.edu.cn (H.L.); syzyclx@163.com (L.C.)

Received: May 26, 2026; Accepted: October 8, 2026; Published Online: October 14, 2026; https://doi.org/10.59717/j.xinn-drugdisc.2026.100046

© 2026 The Author(s). This is an open access article under the CC BY license (https://creativecommons.org/licenses/by/4.0/).

GRAPHICAL ABSTRACT



PUBLIC SUMMARY

- Proteolysis-targeting chimera (PROTAC) proteomics identified PYM1 and ALYREF as celastrol targets.
- Celastrol perturbed exon junction complex–linked nonsense-mediated mRNA decay and promoted G1 arrest.
- Celastrol modulated the ALYREF/FADS2/GPX4 axis and enhanced lipid peroxidation-related redox changes.

ARTICLE Chemical Biology

OPEN ACCESS

Target identification of celastrol based on PROTAC technology and its antitumor mechanism in MDA-MB-231 cells

Man Zhu,[1,3] Haoze Song,[1,3] Yang Liu,[1,2,3] Kuiru Sa,[1] Hongbo Chen,[1] Yueying Yang,[1] Dejuan Sun,[1,*] Hua Li,[2,*] and Lixia Chen[1,*]

[1]Wuya College of Innovation, Key Laboratory of Structure-Based Drug Design & Discovery, Ministry of Education, Shenyang Pharmaceutical University, Shenyang 110016, China

[2]Institute of Digital Materia Medica and Structural Pharmacology, College of Pharmacy, Fujian University of Traditional Chinese Medicine, Fuzhou 350122, China

[3]These authors contributed equally

*Correspondence: sywysdj@163.com (D.S.); lihua@fjtcm.edu.cn (H.L.); syzyclx@163.com (L.C.)

Received: May 26, 2026; Accepted: October 8, 2026; Published Online: October 14, 2026; https://doi.org/10.59717/j.xinn-drugdisc.2026.100046

© 2026 The Author(s). This is an open access article under the CC BY license (https://creativecommons.org/licenses/by/4.0/).

Citation: Zhu M., Song H., Liu Y., et al. (2026). Target identification of celastrol based on PROTAC technology and its antitumor mechanism in MDA-MB-231 cells. *The Innovation Drug Discovery* 1:100046.

Celastrol is a pentacyclic triterpenoid natural product derived from *Tripterygium wilfordii*, known for its significant antitumor activity. However, its specific molecular targets in triple-negative breast cancer (TNBC) remain unclear. This study aimed to identify targets of celastrol using proteolysis-targeting chimera (PROTAC) technology and to verify its antitumor mechanism in MDA-MB-231 cells. The candidate targets PYM1 and ALYREF for celastrol were identified in MDA-MB-231 cells. Microscale thermophoresis (MST), cellular thermal shift assay (CETSA), and drug affinity responsive target stability (DARTS) were used to confirm the binding of celastrol to PYM1 and ALYREF. Mechanistic studies suggested that celastrol interfered with PYM1-associated EJC regulation, accompanied by impaired nucleocytoplasmic cycling of the EJC core components Y14 and MAGOH. This perturbation was associated with suppression of nonsense-mediated mRNA decay (NMD)-related mRNA surveillance, partial activation of p53/p21 signaling, and G1 phase cell cycle arrest in MDA-MB-231 cells. In addition, celastrol modulated the ALYREF/FADS2/GPX4 axis and increased MDA accumulation, suggesting a potential involvement of this axis in lipid peroxidation-related redox changes in MDA-MB-231 cells. These findings provide new insights into the pharmacological mechanisms of celastrol and may contribute to innovative therapeutic strategies for triple-negative breast cancer.

INTRODUCTION

Celastrol, also known as tripterine, is a triterpenoid compound with excellent antitumor activity. In recent years, multiple methods have been employed to identify the targets of celastrol, including chemical probes, mass spectrometry analysis, *etc.*[1-3] A previous study used the OTTER (omics and text-based target enrichment and ranking) method to identify differentially expressed genes from omics data after celastrol treatment, determining the covalent binding target protein PRDX1 of celastrol.[4] It has also been reported that multiple targets of celastrol, including Hsp90β and PRDX1, were identified using the CGCP (chemical genomics-facilitated chemical proteomics) technology.[5] Yang *et al.* identified YY1 and HMCES as the targets of celastrol using the MS-CETSA method.[6] Quantitative chemical proteomics was used to discover that the target of celastrol in the ischemia-reperfusion model is HMGB1.[7] Luo *et al.* identified potential anti-hepatocellular carcinoma targets of celastrol by activity-based protein profiling (ABPP) and found that celastrol selectively targeted voltage-dependent anion channel 2.[8] Multi-omics analysis combined with molecular docking and CETSA was used to verify the direct target protein P5CDH of celastrol in inhibiting drug-resistant Staphylococcus aureus.[9] Zhu *et al.* used the Target-Responsive Accessibility Profiling (TRAP) approach to probe lysine accessibility changes at the proteome level and identified CAP1 as a binding protein of celastrol.[10] Multi-technique integration identified PCAF as celastrol's direct target, suppressing TGF-β-induced epithelial-mesenchymal transition and pulmonary fibrosis via PCAF/NF-κB axis inhibition.[11] The methods mentioned above have certain limitations, such as high affinity dependence, non-specific binding and complex experimental procedure. So, it is essential to explore novel supplementary approaches to identify the targets of celastrol.

We develop PROTAC technology as an innovative approach for the target identification of natural products. Our research team has identified MAFF as the target protein of Lathyrol using PROTAC-based target identification technology for the first time.[12] PROTACs do not require strong binding but rely on the formation of a ternary complex involving the target-PROTAC-E3 ligase. The event-driven mechanism of action of PROTACs offers several advantages compared to traditional occupancy-driven small molecule inhibitors, including high selectivity, sustained effects, reduced resistance, and the ability to target hard-to-inhibit proteins.[13-15]

Breast cancer remains one of the most prevalent malignancies and a major global health burden, while triple-negative breast cancer (TNBC) represents a particularly aggressive subtype with limited therapeutic options.[16] Research indicates that celastrol can inhibit TNBC cell proliferation and metastasis through multiple molecular pathways.[17-18] However, its specific molecular targets in TNBC remain unclear. It is crucial to validate the target of celastrol, providing a theoretical foundation for subsequent drug development and enhancing the therapeutic efficacy of TNBC.

In this study, we aimed to identify candidate targets of celastrol using PROTAC technology and to verify its target-related antitumor mechanism in MDA-MB-231 cells. Eighteen celastrol-based PROTACs containing six E3 ubiquitin ligase ligands were designed and synthesized, followed by proteomics analysis to identify candidate celastrol-associated targets. Guided by the proteomic results, PYM1 and ALYREF were selected as candidate targets for subsequent validation. Target binding assays and functional studies were then performed to investigate the possible roles of these candidates in the antitumor effects of celastrol in TNBC cells. This study provides a PROTAC-based strategy for exploring the molecular targets of celastrol and offers new insights into its antitumor mechanisms in TNBC cells.

MATERIALS AND METHODS

Chemistry and synthesis

Reactions were monitored by thin-layer chromatography (TLC) analysis, which was performed on glass plates precoated with silica gel (GF-254), and visualized by UV fluorescence (λ_{max} = 254 nm). Products were purified by flash column chromatography, which was performed using silica gel (200-300 mesh). ^{1}H NMR spectra were obtained on 400 or 600 MHz Bruker AVANCE spectrometer, and ^{13}C NMR spectra were obtained on 101 or 151 MHz Bruker AVANCE spectrometer (Bruker Instruments Inc. Germany). Chemical shifts for ^{1}H NMR spectra are reported in parts per million (ppm) from tetramethylsilane with the solvent resonance as the internal standard ($CDCl_3$, 7.26 ppm; DMSO-d_6, 2.50 ppm). Data are reported as follows: chemical shift, multiplicity (s = singlet, d = doublet, t = triplet, q = quartet, p = quintet, m = multiplet, br = broad), coupling constants (Hz), and integration. A high-resolution mass spectrum (HRMS) was measured on a FLEX-PC (ultraflex TOF/TOF) instrument equipped with an atmospheric pressure chemical ionization (APCI) or electrospray ionization (ESI) source in the positive-ion mode. Detailed reaction condition information and characterization data were provided in the Supplemental methods 1.1-1.7 and Supplemental section 4 Copies of compounds NMR and HRMS spectra.

Cell culture

Human triple-negative breast cancer MDA-MB-231 cells were obtained from Procell and cultured in Dulbecco's Modified Eagle Medium (DMEM, Procell) supplemented with 10% (v/v) fetal bovine serum (FBS) and 1% (v/v) Penicillin-Streptomycin Solution at 37 °C with 5% CO_2. For all experimental handling of PROTAC, unless otherwise stated, cells were co-incubated with chemicals for 24 hours. For ubiquitin proteasome inhibition assays, cells were

pre-treated with MG132 (MCE, HY13259) for 2 hours followed by co-incubation with PROTAC for 24 hours. For ligand competitive experiments, cells were pre-treated with celastrol or Nutlin carboxylic acid for 2 hours followed by co-incubation with PROTAC for 24 hours. For all cell-based experiments, the vehicle control group was treated with an equal volume of DMSO corresponding to the highest drug concentration used in each experiment, and the final DMSO concentration did not exceed 0.1% (v/v) in both control and drug-treated groups unless otherwise stated.

Cell viability assay

Cell viability was detected by Cell Counting Kit-8 (CCK-8) assay (TargetMol, USA). MDA-MB-231 cells were seeded in 96-well plates for 12 hours, then treated with celastrol and PROTACs at various concentrations for 24 hours. CCK-8 reagent was added, and cells were incubated at 37 °C in the dark for 30-60 min before measuring the absorbance at 450 nm with a microplate reader.

Proteomic mass spectrometry analysis

MDA-MB-231 cells were independently prepared as biological replicates (n = 3) and divided into five groups: DMSO control, celastrol, PROTAC_4, PROTAC_9, and PROTAC_18. After treatment for 24 h, cells were collected, lysed, and subjected to protein extraction, trypsin digestion, and TMT labeling according to previously described protocols.[19-20] Three biological replicates from each group were analyzed using a 6-plex TMT labeling kit. Five TMT channels were assigned to the five experimental groups, and the labeled peptides were analyzed by LC-MS/MS using a Q Exactive Plus mass spectrometer.

Raw MS/MS data were searched against the UniProt human protein database using Mascot software (version 2.3.0). Protein quantification was based on TMT reporter ion intensities, and data normalization and differential protein analysis were performed using established proteomic data processing workflows.

Target protein data analysis

Protein abundance changes were analyzed based on the TMT protein intensities of the negative control, celastrol and PROTAC-treated groups, including PROTAC_4, PROTAC_9 and PROTAC_18. Differentially abundant proteins were first annotated using fold change < 0.667 or > 1.5 with $p < 0.05$ as the cutoff. For PROTAC-assisted target discovery, only significantly down-regulated proteins were considered. Candidate targets were defined as proteins that met the following criteria: (i) significantly reduced by both PROTAC_4 and PROTAC_9, (ii) not significantly reduced by celastrol alone under the same cutoff, and (iii) supported by reliable MS identification parameters, defined as identification with at least two unique peptides. Peptide number and sequence coverage were further used as supporting parameters to evaluate MS identification confidence and to prioritize candidate targets. The detailed peptide number, unique peptide number, and sequence coverage values are provided in Table S3. The resulting candidates were further prioritized according to degradation magnitude and biological relevance. Selected proteins were subjected to the heatmap, Volcano plots, Venn and GO enrichment analysis.

Immunoblotting (IB) assay

Protein expression was analyzed by western blotting according to standard protocols. A complete list of antibodies and detailed procedures are provided in the Supplemental methods 1.8.

Quantitative real-time PCR (RT-qPCR) assay

Total mRNA was extracted using TRIzol (Sigma-Aldrich, #T9424) according to the manufacturer's instructions. Then, cDNA was synthesized from 0.1 μg of mRNA using the HiScript II RT SuperMix for qPCR (Vazyme, #R323-01). Real-time quantitative PCR (RT-qPCR) was performed using ChamQ Universal SYBR qPCR Master Mix (Vazyme, #Q711-02). The GAPDH gene was used to normalize relative mRNA levels. The primer list can be found in Table S2.

Microscale thermophoresis assay

Microscale thermophoresis assay was conducted following the methodology previously employed in our research.[8] Detailed procedures are described in the Supplemental methods 1.9.

Cellular thermal shift assay (CETSA)

MDA-MB-231 cell lysates were treated with 10 μM celastrol (for protein PYM1) and 3 μM celastrol (for protein ALYREF) or vehicle control DMSO at a final concentration of 0.02% (v/v) at 37 °C for 1 hour. The lysates were then divided into different aliquots and heated at temperatures ranging from 78 to 88 °C (for protein PYM1) or from 67 to 72 °C (for protein ALYREF) for 15 minutes, followed by centrifugation at 12000 g for 10 minutes. The supernatant was collected for further immunoblotting analysis.

Drug affinity responsive target stability (DARTS) assay

MDA-MB-231 cell lysates were divided into a negative control group, a pronase-digestion control group and celastrol treatment groups (2.5 μM, 5 μM, 10 μM, 20 μM for protein PYM1 and 1.5 μM, 3 μM, 6 μM for protein ALYREF). Celastrol at the indicated concentrations or an equal volume of DMSO (0.08%, v/v) was added to the lysates, which were then incubated at 37 °C for 1 hour. Then, enzyme digestion and treatment groups were supplemented with 1:200 diluted pronase E (Sigma-Aldrich, #P5147), the negative control group was added with an equal volume of PBS. After mixing, the samples were incubated at 37 °C for 20 minutes. The reaction was terminated by adding sample buffer and boiling for 5 minutes. The samples were then analyzed by immunoblotting.

Co-Immunoprecipitation (Co-IP) analysis

For endogenous co-immunoprecipitation, MDA-MB-231 cell lysates were obtained in IP cell lysis buffer (Beyotime, #P0013) supplemented with 1 mM PMSF. Subsequently, cell lysates were incubated with 1 μg of specific antibody overnight at 4 °C on a rotator, by incubation with 20 μL of Protein A+G agarose beads for 4 hours. The IP complexes were washed five times with PBS and eluted in sample buffer (50 mM Tris-HCl, pH 6.9, 2% SDS, 10% glycerol, 100 mM DTT and 0.1% bromophenol blue) for 5 minutes. The samples were then subjected to SDS-PAGE for immunoblot analysis.

Immunofluorescence (IF) assay

Cellular localization of target proteins was assessed by immunofluorescence. Detailed information on antibodies, dilution ratios, and imaging settings can be found in the Supplemental methods 1.10.

Plasmid transfection assay

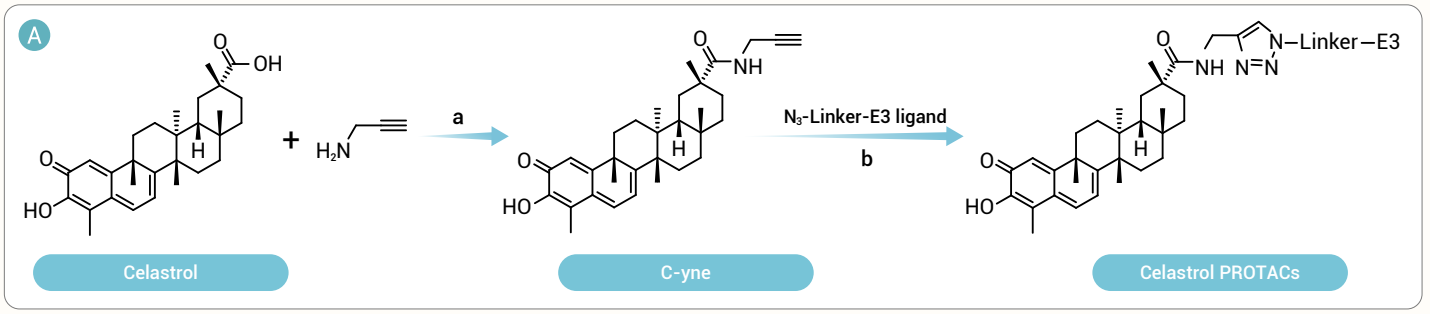
Plasmids encoding short hairpin RNAs targeting human PYM1 (shPYM1; #P57873) and ALYREF (shALYREF; #P52931) were purchased from the Miao Ling Plasmid Platform. Overexpression plasmids for Y14 protein (Y14 OP) were obtained from Miao Ling Plasmid Platform (#P54293). MDA-MB-231 cells were transfected using Hieff Trans™ Liposomal Transfection Reagent (YEASEN, #4080203) according to the manufacturer's instructions. After 48 hours post-transfection, cells were used for RT-qPCR, immunofluorescence, cell cycle analysis and immunoblotting assays.

Nucleocytoplasmic fractionation and ribosome protein isolation

For nucleocytoplasmic fractionation, extraction was performed by using the CER-NER kit (Meilunbio, #0211). For ribosome protein isolation, the ribosome protein extraction kit (Best, #BB-3142) was used to extract the ribosome protein. Protein concentrations were measured by using the BCA assay kit (Beyotime, #P0012), and the samples were subsequently analyzed by immunoblotting.

Cell cycle analysis

Cell cycle was measured using the Cell Cycle and Apoptosis Analysis Kit (Beyotime, #1052). MDA-MB-231 cells (1×10^5 cells/mL, 2 mL) were seeded in six-well plates. After treatment, cells were fixed overnight at 4 °C in cold 70% ethanol. Cells were incubated with propidium iodide working solution containing 10 μL RNase A at 37 °C for 30 minutes. Samples were analyzed using the FACSCelesta flow cytometer (Becton Dickinson CA) at 488/575 nm excitation/emission wavelengths, and 10000 cells were collected for each sample.



B

Compound	E3 ligase	E3 ligase ligand	IC_{50} (μM) (MDA-MB-231)
Celastrol	/	/	2.84 ± 0.31
1	cIAP	B4	26.56 ± 2.14
2	cIAP	B4	-
3	cIAP	B4	-
4	cIAP	B5	10.57 ± 1.07
5	cIAP	B5	43.13 ± 4.45
6	cIAP	B5	22.48 ± 3.08
7	MDM2	Nutlin-3	-
8	MDM2	Nutlin-3	-
9	MDM2	Nutlin-3	11.79 ± 1.07
10	VHL	V1	-
11	VHL	V1	-
12	VHL	V1	-
13	VHL	V2	-
14	VHL	V2	-
15	VHL	V2	-
16	CRBN	Thalidomide 4-fluoride	20.36 ± 5.58
17	CRBN	Thalidomide 4-fluoride	16.41 ± 6.77
18	CRBN	Thalidomide 4-fluoride	4.93 ± 1.19

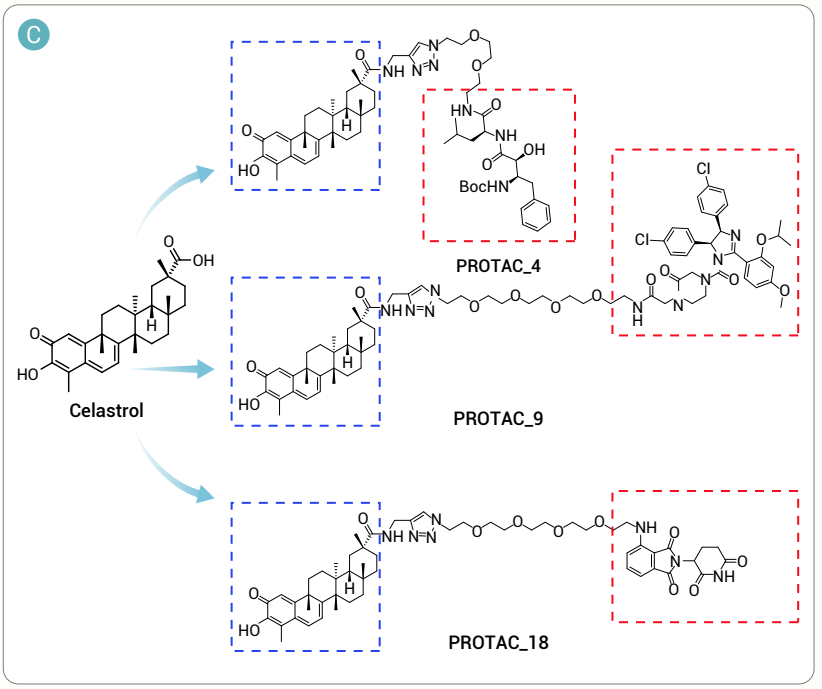


Figure 1. The synthesis of celastrol PROTACs and *in vitro* proliferation inhibition in MDA-MB-231 cells of PROTAC library based on celastrol (A) The synthesis of celastrol PROTACs. Reagents and conditions: (a) EDCI, HOBt, DIPEA, DCM, 0 °C to rt., 2 hours. (b) $CuSO_4$, Sodium *L*-Ascorbate, THF/H_2O, rt., 0.5 hours. (B) Summary of IC_{50} values on MDA-MB-231 cells for PROTAC library. "-" indicates no significant inhibitory activity. (C) The structures of celastrol, PROTAC_4, PROTAC_9 and PROTAC_18. Representative results from three independent experiments are shown. Data are presented as mean ± SEM, n = 3.

Measurement of malondialdehyde (MDA) levels

MDA levels were assessed using specific assay kits. MDA-MB-231 cells were seeded in 6-well plates at a density of 5×10^5 cells per well. Following cell adhesion, the cells were treated with different concentrations of celastrol (0, 1.5, 3 and 6 μM) for 24 hours. The 0 μM group was treated with DMSO vehicle control, and the final DMSO concentration was 0.02% (v/v). After treatment, cells were collected and lysed according to the manufacturer's instructions for the MDA assay kit (Beyotime, S0131S). The samples were centrifuged, and 100 μL of the sample supernatant from each group was collected in a 96-well plate. The absorbance of each well at 532 nm was detected using a microplate reader. MDA levels were calculated according to the manufacturer's instructions.

Molecular docking analysis

Molecular docking analysis was performed to predict the possible binding mode between celastrol and 21 candidate proteins with available suitable structures. The three-dimensional structures of proteins were obtained from the Protein Data Bank (Table S3), and the structure of celastrol was prepared before docking. Protein preparation, ligand preparation, and docking analysis were performed using Autodock software (Autodock Tools 1.5.7) according to the standard protocol. The docking pose with a favorable binding score and reasonable interaction mode was selected for visualization.

Statistical analysis

Experimental data were statistically analyzed using GraphPad Prism 8.0, Excel, and SPSS software. All data are presented as mean ± SEM from at least three independent experiments. Data distribution was assessed before statistical analysis. For comparisons between two groups, an unpaired two-tailed Student's t-test was used for normally distributed data. For comparisons among three or more groups, one-way analysis of variance (one-way ANOVA) followed by Tukey's multiple comparisons test was performed. p value < 0.05 was considered statistically significant.

RESULTS

Design, synthesis and evaluation of celastrol-based PROTACs

We designed and synthesized 18 PROTACs with six E3 ubiquitin ligase ligands known to recruit Cereblon (CRBN), murine double minute 2 (MDM2), von Hippel-Lindau (VHL), and cellular inhibitor of apoptosis (cIAP). For synthesizing the PROTACs of celastrol, two kinds of linkers (polyethylene glycol (PEG, referred to as P) and carbon chains (referred to as C)) were selected. Considering the effect of the linker length on the physicochemical and pharmacokinetic properties, as well as the binding activity of PROTACs, we chose six linker variants (2P, 3P, 4P, 1C, 3C, 5C) as the connecting arm.[13] Meanwhile, six E3 ligase ligands corresponding to four E3 ligases, Thalidomide 4-fluoride (CRBN ligand), Nutlin-3 (MDM2 ligand), VH032 including VHL1 and VHL2 (VHL ligand), B4 and B5 (cIAP ligand) were selected to evaluate the impact of different E3 ligases on PROTAC degradation activity.[13,21] Table S1 shows the structures of N_3-Linker-E3 compounds. Figure 1A exhibits the synthesis of celastrol PROTACs. Initially, celastrol reacted with propargylamine to obtain alkyne intermediates. It was confirmed through

HMBC and HSQC that propargylamine reacted at the carboxyl position of celastrol. Then, the classical copper-catalyzed azide-alkyne cycloaddition of azides and alkynes assembled the warhead intermediates, linkers, and E3 ligase ligands into a series of PROTAC molecules. A total of 18 celastrol PROTACs were synthesized (Figure S1).

The proliferation inhibition of celastrol and the PROTAC molecules against MDA-MB-231 cells was evaluated. PROTAC_4, PROTAC_9 and PROTAC_18 exhibited the strongest activity among all the synthesized compounds (Figure 1B). Therefore, PROTAC_4, PROTAC_9 and PROTAC_18 were selected as the PROTAC tool molecules for subsequent target identification studies (Figure 1C).

Target identification of celastrol by PROTAC technology in MDA-MB-231 cells

Differential proteomics analysis based on TMT tandem mass spectrometry was conducted to assess protein abundance changes in MDA-MB-231 cells treated with celastrol, PROTAC_4, PROTAC_9, PROTAC_18 or DMSO for 24 h (Figure 2A). For PROTAC-assisted target discovery, significantly downregulated proteins were screened using a uniform cutoff of fold change < 0.667 and $p < 0.05$. To reduce the interference from proteins regulated by celastrol treatment itself, proteins significantly decreased in the celastrol group under the same cutoff were excluded from subsequent candidate target selection. Under this criterion, PROTAC_4 and PROTAC_9 induced significant downregulation of 79 and 82 proteins, respectively. Although PROTAC_18 showed relatively strong antiproliferative activity, it resulted in a limited number of significantly downregulated proteins in the TMT-based proteomic analysis (Table S3, Figure S2). Therefore, PROTAC_4 and PROTAC_9 were used as the major tool molecules for convergence-based target screening.

The intersection of proteins significantly reduced by both PROTAC_4 and PROTAC_9 yielded 51 candidate proteins after excluding proteins decreased by celastrol alone. To evaluate the biological relevance of these candidates, GO annotation, KEGG pathway enrichment, protein-protein interaction (PPI) analysis and COG/KOG functional classification were performed (Figure 3A-D). These analyses suggested that several candidates were associated with RNA processing, ribosome-related regulation, nucleocytoplasmic transport and post-transcriptional control, providing a rationale for prioritizing RNA metabolism-associated proteins. The 51 candidates were then ranked according to reproducible degradation by two independent PROTAC molecules, MS identification confidence, peptide coverage and biological relevance. Among them, PYM1 showed the strongest degradation, with PROTAC_4/Control and PROTAC_9/Control ratios of 0.399 and 0.288, respectively, and was identified with 40.2% sequence coverage and six unique peptides. Functionally, PYM1 is related to EJC disassembly and NMD-associated mRNA surveillance. ALYREF was also reproducibly reduced by both PROTAC_4 and PROTAC_9, with ratios of 0.597 and 0.437, respectively, and was supported by 40.5% sequence coverage and eight unique peptides. Given its role as an mRNA export adaptor involved in RNA processing and nucleocytoplasmic transport, ALYREF was also selected for further validation. Therefore, based on the consistency of degradation induced by the two PROTACs, MS identification confidence, degradation magnitude, and biological relevance to RNA metabolism, PYM1 and ALYREF were prioritized from the 51 candidate proteins for focused validation in MDA-MB-231 cells.

To validate the results of the proteomic analysis, we first conducted degradation activity assays on the PYM1 candidate target protein treated with PROTAC_9. The results showed that PROTAC_9 degraded PYM1 protein in a concentration and time-dependent manner (Figure 2C-D). The degradation of PYM1 was blocked by the proteasome inhibitor MG132 (Figure 2E). High concentrations of celastrol and Nutlin carboxylic acid can both compete with PROTAC_9 to block the degradation of PYM1 (Figure 2F). These results suggest that the degradation of PYM1 by PROTAC_9 depends on the ubiquitin-proteasome system. Direct interaction between celastrol and PYM1 was also detected using MST, CETSA and DARTS assays. The MST assay showed that celastrol bound to PYM1 with a dissociation constant (Kd) of 14.38 μM (Figure 2G). The results of CETSA assay indicated that celastrol significantly increased the thermal stability of PYM1 protein compared to the DMSO group (Figure 2H). DARTS results also showed that celastrol could dose-dependently enhance PYM1 resistance to pronase hydrolysis (Figure 2I). Collectively, these results suggest that PYM1 is a potential target of celastrol in MDA-MB-231 cells.

Celastrol disrupts the cytoplasmic-nuclear cycling of Y14 and MAGOH, thereby interfering with EJC function

Exon junction complex (EJC) is a multi-protein assembly comprised of essential core proteins, including Y14, MAGOH, eIF4A3, and MLN51. This complex plays a critical role in post-splicing mRNA processing. EJC facilitates mRNA transport to the cytoplasm by interacting with other nucleoplasmic transport factors. PYM1, which is located in the cytoplasm, serves as a crucial dissociation factor for the EJC, facilitating the release of the MAGOH-Y14 complex and its subsequent entry into the nucleus to re-participate in EJC assembly.[22-23] The result of immunoprecipitation assay showed that celastrol significantly inhibited the interaction between PYM1 and Y14/MAGOH (Figure 4A). In addition, celastrol blocked Y14-MAGOH complex entry into nucleus and did not significantly affect the total protein levels of Y14 and MAGOH in MDA-MB-231 cells (Figure 4B-C). To further investigate whether celastrol inhibits the cytoplasmic-nuclear cycling of Y14 and MAGOH through PYM1, we knocked down PYM1 expression in MDA-MB-231 cells by transfecting shRNA plasmids (shPYM1) (Figure S3). Compared with wild-type (WT) cells, PYM1 knockdown attenuated the additional effect of celastrol on Y14-MAGOH redistribution (Figure 4D), suggesting that PYM1 is involved in celastrol-associated disruption of Y14/MAGOH nucleocytoplasmic cycling.

Nonsense-mediated mRNA decay (NMD) is a process during which PYM1 typically binds to the 40S ribosomal subunit and disassembles the EJC during the first round of translation, allowing the core proteins MAGOH and Y14 to dissociate from mRNA and recycle back to the nucleus.[24] We sought to explore how celastrol interferes with the function of PYM1 leading to the retention of Y14 and MAGOH on the ribosomes. The results indicated that celastrol did not interfere with the attachment of PYM1 on the ribosomes. Conversely, it significantly increased the levels of Y14 and MAGOH in the ribosomes. This effect was substantially diminished when PYM1 was knocked down (Figure S4). The results of immunofluorescence also showed that after treatment with celastrol, the co-localization of Y14 and MAGOH with RPS3 was significantly increased (Figure 4E-F). After knocking down PYM1, the co-localization of RPS3 with Y14 and MAGOH was significantly reduced (Figure 4G-H). These results suggest that celastrol perturbs PYM1-associated EJC dynamics, leading to increased ribosome-associated retention of Y14 and MAGOH and impaired recycling of EJC core components. This caused the improper accumulation of Y14 and MAGOH in the cytoplasm, interfering with mRNA translation and decreasing its efficiency.

Celastrol perturbs PYM1-associated EJC/NMD regulation and promotes G1 phase cell cycle arrest in MDA-MB-231 cells

NMD is a highly conserved RNA regulatory pathway that selectively degrades mRNA containing premature termination codons (PTCs), resulting in nonsense mutations, frameshift mutations, and splice site mutations.[25] EJC is an important component involved in NMD. During translation, the ribosome typically removes EJC, but if EJC is located downstream of PTCs, EJC remains on the mRNA and serves as a signal to recruit NMD factors and induce NMD process of the mRNA.[26-27] The degradation of abnormal p53 mRNA through the NMD process causes a loss of tumor-suppressive functions.[28] To investigate whether celastrol affects the NMD process in MDA-MB-231 cells through PYM1, we selected three known NMD substrates (SC35, ASNS, and CARS) to evaluate their degradation in the presence of celastrol.[24,29-30] RT-qPCR results indicated that the mRNA levels of these substrates significantly increased after celastrol treatment, suggesting that celastrol inhibited the NMD process in MDA-MB-231 cells (Figure 5A). After knocking down PYM1, the impact of celastrol on NMD significantly decreased (Figure 5B).

Then we investigated whether celastrol affects the expression of p53 in MDA-MB-231 cells. The results showed that celastrol upregulated the levels of p53 and p21 in a concentration-dependent manner, with no significant effect on the protein level of MDM2 (Figure 5C). However, knocking down PYM1 blocked the upregulation of p53 and p21 induced by celastrol (Figure

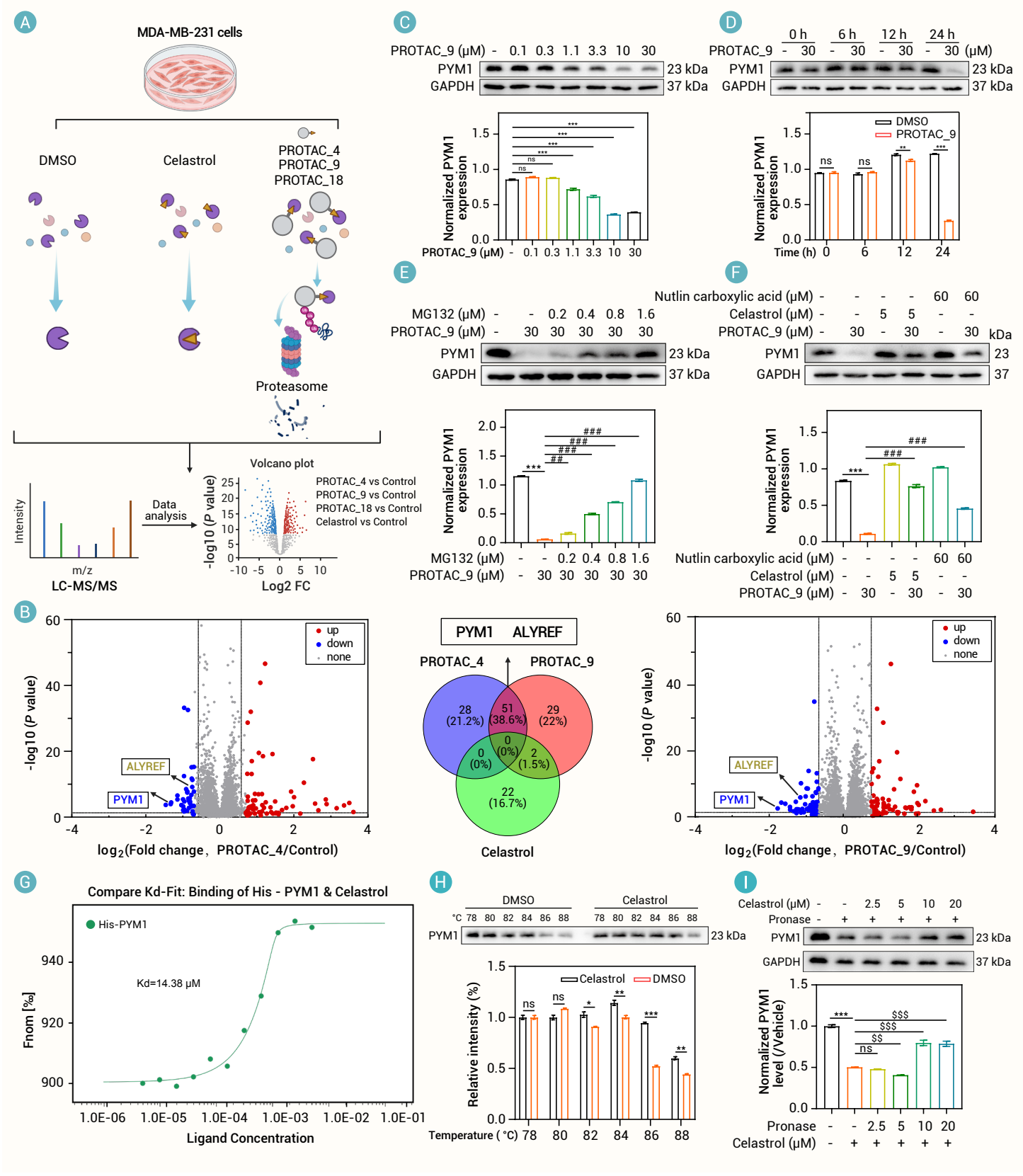


Figure 2. Target identification of celastrol by PROTAC in MDA-MB-231 cells (A) A TMT-based mass spectrometry (MS) approach was used to assess the proteome changes in MDA-MB-231 cells after 24 hours treatment of DMSO, celastrol, PROTAC_4, PROTAC_9 and PROTAC_18. (B) Volcano plot displays Differentially Expressed Proteins (DEPs) of PROTAC_4/ Control (left panel) and PROTAC_9/Control (right panel) in MDA-MB-231 cells. The differential target proteins were selected on the basis of the fold change < 0.667 (down-regulated), fold change >1.5 (up-regulated) and *p* value < 0.05. Up-regulated proteins are colored in red. Down-regulated proteins are colored in blue, and non-significantly changed proteins are colored in gray. Venn diagram of overlapping significantly changed proteins (middle panel). (C) PROTAC_9 degraded the PYM1 protein in a concentration-dependent manner. (D) PROTAC_9 degraded the PYM1 protein in a time-dependent manner. (E) The reversal of PROTAC_9 degradation activity by MG132 in MDA-MB-231 cells. (F) The competitive inhibition of degradation activity of PROTAC_9 by celastrol and Nutlin carboxylic acid. (G) MST experiments were conducted to determine the binding affinity between celastrol and PYM1. (H) CETSA assay was performed to evaluate the effect of celastrol on PYM1 thermal stability. (I) DARTS assay was performed to assess the effect of celastrol on PYM1 resistance to pronase digestion. Data are presented as mean ± SEM. $^{*}p < 0.05$, $^{**}p < 0.01$, $^{***}p < 0.001$ vs. the DMSO group. $^{\#\#}p < 0.01$, $^{\#\#\#}p < 0.001$ vs. the PROTAC_9 group. $^{\$\$}p < 0.01$, $^{\$\$\$}p < 0.001$ vs. the Pronase group. ns, no significance.



Figure 3. Degradation proteomics was used to identify the target of celastrol in MDA-MB-231 cells (A) Statistical distribution chart of identified DAPs between celastrol group and negative control group based on GO category. The bar represents the number of DAPs. (B) KEGG analysis highlights the DAPs of celastrol group vs. negative group in MDA-MB-231 cells. (C) Protein–protein interaction network identified among celastrol group vs. negative control group using STRING database. (D) COG/KOG functional classification chart of the identified DAPs between celastrol group and negative control group in MDA-MB-231 cells. (E) The DAPs with significant difference were clustered in this map. The X-axis represented the samples, and the Y-axis represented the differential gene names. Red represented the highly expression, and blue represented the lowly expression.

5D). Previous studies have found that inhibiting NMD significantly upregulates p53β and p53γ, thereby partially reactivating p53-associated signaling.[31] Our results showed that celastrol significantly increased the mRNA levels of p53β and p53γ. Additionally, the knockdown of PYM1 partially interrupted this

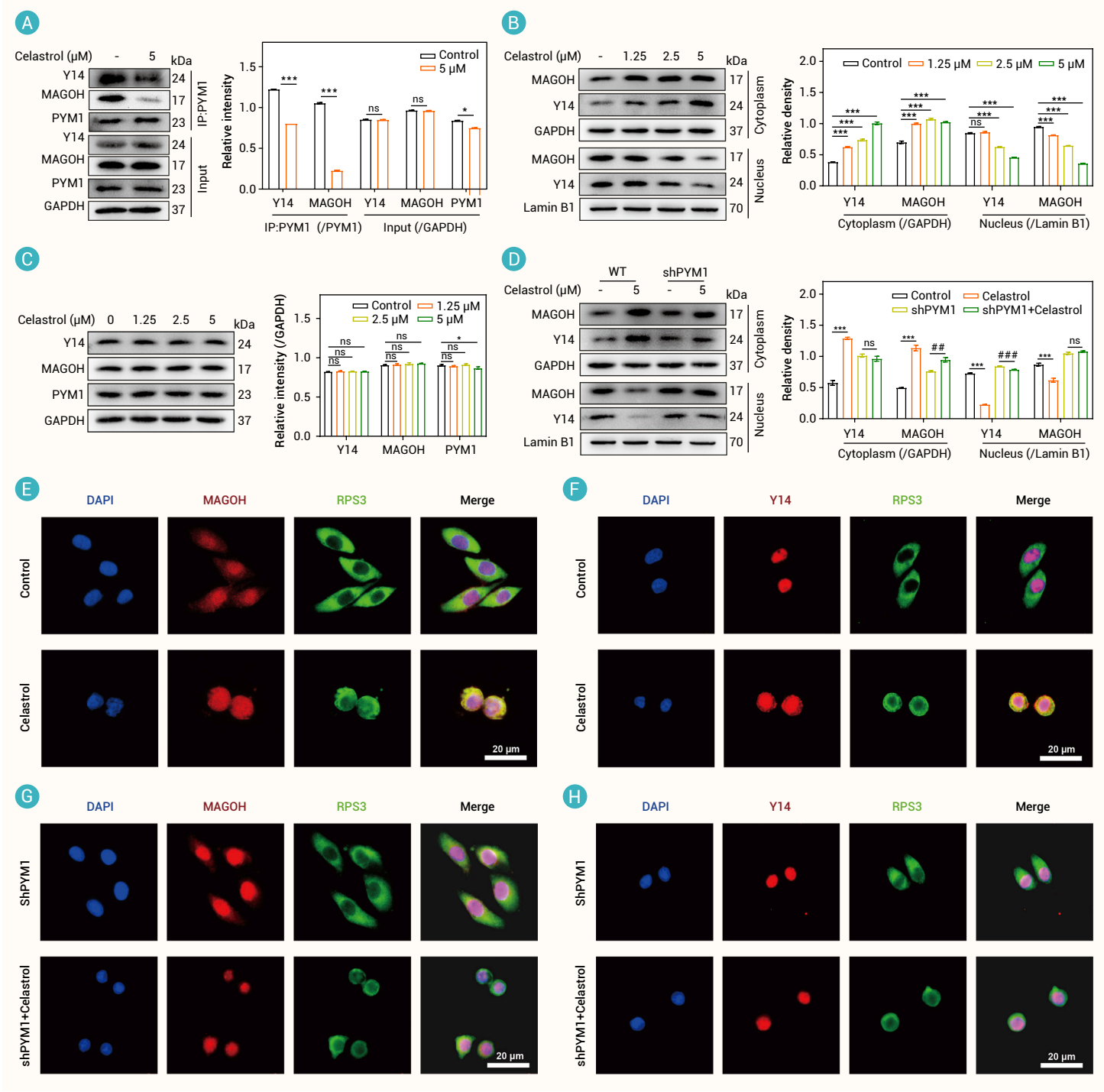


Figure 4. Celastrol disrupts the cellular cycle of Y14 and MAGOH, interfering with EJC function (A) The co-immunoprecipitation (co-IP) experiment evaluating the interaction between PYM1 and Y14-MAGOH. (B) The distribution of Y14-MAGOH between the cytoplasm and nucleus. (C) The changes in the total protein levels of Y14-MAGOH within the cells. (D) The variations in the levels of Y14-MAGOH between the cytoplasm and nucleus in the WT and shPYM1 cell. (E-F) The co-localization of MAGOH (E) and Y14 (F) with RPS3 in WT cells after treatment with celastrol for 12 hours. (G-H) The co-localization of MAGOH (G) and Y14 (H) with RPS3 in shPYM1 cells after treatment with celastrol for 12 hours. Y14/MAGOH was colored in red. RPS3 was colored in green. Nuclei were labeled with DAPI (blue). Scale bar, 20 μm. Data are presented as mean ± SEM. $^{*}p < 0.05$, $^{**}p < 0.01$, $^{***}p < 0.001$ vs. the DMSO group. $^{\#\#}p < 0.01$, $^{\#\#\#}p < 0.001$ vs. the shPYM1 group. ns, no significance. The DMSO group served as the vehicle control, and the final DMSO concentration was 0.02% (v/v).

process, which suggested that celastrol was associated with partial activation of p53/p21 signaling in MDA-MB-231 cells, accompanied by changes in NMD-associated transcripts (Figure 5E). Additionally, we investigated whether celastrol affected cell cycle arrest in MDA-MB-231 cells. The results showed that celastrol could downregulate the levels of CDK4 and Cyclin D1, leading to cell cycle arrest at G1 phase. However, knockdown of PYM1 partially blocked this process (Figure 5F-G). Together, these results support that celastrol perturbs PYM1-associated EJC/NMD regulation, thereby contributing to p53/p21 signaling activation and G1 phase cell cycle arrest in MDA-MB-231 cells.

Y14 overexpression partially attenuates celastrol-induced NMD-associated changes

We observed that celastrol increased cytoplasmic retention of Y14, which was associated with PYM1-related EJC dysregulation. This mislocalization led to the inactivation of Y14 and interfered with the cellular NMD process.

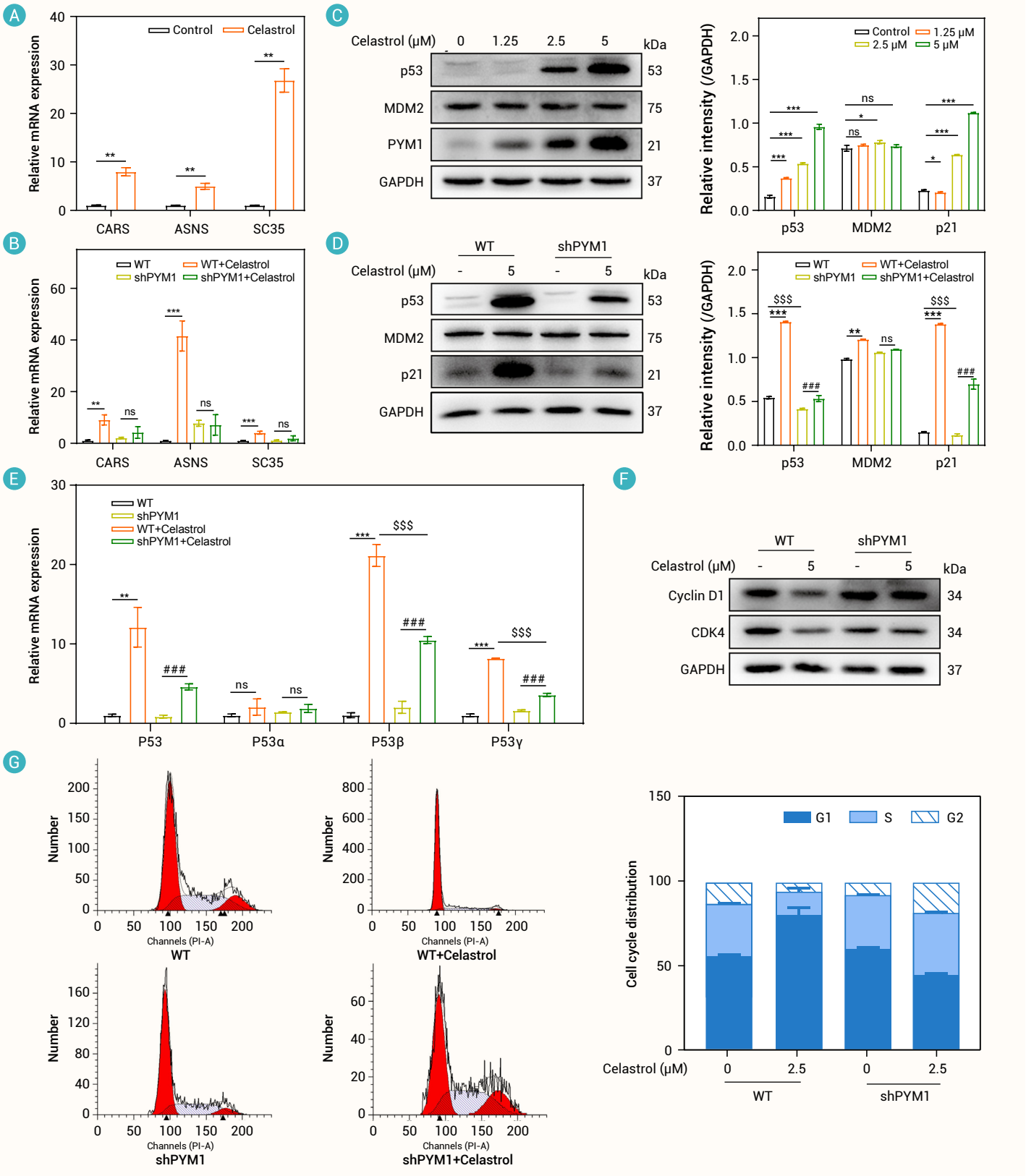


Figure 5. Celastrol perturbs PYM1-associated EJC/NMD regulation and promotes G1 phase cell cycle arrest in MDA-MB-231 cells (A-B) Changes in the abundance of three NMD-responsive transcripts after celastrol treatment in control and PYM1-knockdown cells. (C) The impact of celastrol on p53 expression in MDA-MB-231 cells. (D) Knockdown of PYM1 could partially block the upregulation of p53 caused by celastrol. (E) The influence of celastrol on p53β and p53γ mRNA levels in WT and shPYM1 MDA-MB-231 cells. (F) The regulation of celastrol on cell cycle arrest in WT and shPYM1 MDA-MB-231 cells. (G) Flow cytometry analysis of how celastrol regulated the cell cycle process in WT and shPYM1 MDA-MB-231 cells. Data are presented as mean ± SEM. $^{*}p < 0.05$, $^{**}p < 0.01$, $^{***}p < 0.001$ vs. the DMSO group. $^{\#\#\#}p < 0.001$ vs. the shPYM1 group. $^{\$\$\$}p < 0.001$ vs. the WT + celastrol group. ns, no significance. The DMSO group served as the vehicle control, and the final DMSO concentration was 0.02% (v/v).

Therefore, we hypothesize that overexpression of Y14 may rescue the function of the EJC and reduce the interference of celastrol on the NMD process. After the overexpression of Y14, the transcription levels of the three NMD substrates significantly decreased, and the inhibition of NMD induced by

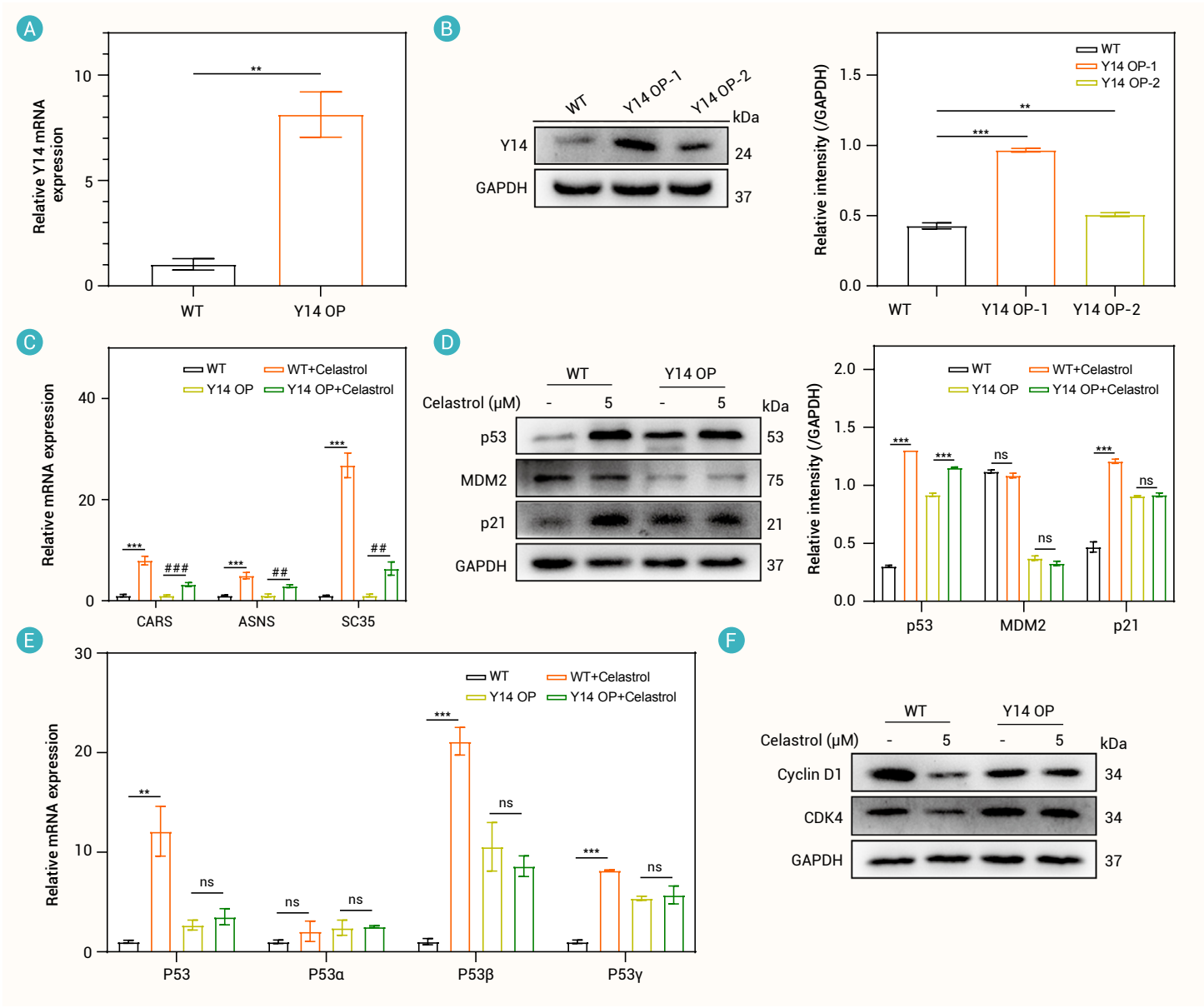


Figure 6. Y14 overexpression partially attenuates celastrol-induced NMD-associated changes (A) RT-qPCR detected the mRNA levels of Y14 in WT and Y14 OP (Y14 overexpression) MDA-MB-231 cells. (B) Western blotting analysis of Y14 expression in WT cells and two preliminary Y14 overexpression conditions (Y14 OP-1 and Y14 OP-2). Based on the higher Y14 expression level, Y14 OP-1 was selected for subsequent experiments. (C) RT-qPCR analysis of NMD substrate transcripts in WT and Y14 OP cells after celastrol treatment. (D) Effects of Y14 overexpression on celastrol-induced changes in p53, MDM2 and p21 protein levels. (E) RT-qPCR analysis of p53 and TP53 isoform mRNA levels after Y14 overexpression and celastrol treatment. (F) Western blotting analysis of Cyclin D1 and CDK4 protein levels in WT and Y14 OP cells after celastrol treatment. Data are presented as mean ± SEM. $^{**}p < 0.01$, $^{***}p < 0.001$ vs. the DMSO group. $^{\#\#}p < 0.01$, $^{\#\#\#}p < 0.001$ vs. the Y14 OP group. ns, no significance. The DMSO group served as the vehicle control, and the final DMSO concentration was 0.02% (v/v).

celastrol was partially restored (Figure 6A-C). Similarly, Y14 overexpression also partially blocked the increase in p53 protein levels caused by celastrol and partially reversed the upregulation of the p53β and p53γ isoforms (Figure 6D-E). Furthermore, Y14 overexpression partially reversed the celastrol-induced reduction of Cyclin D1 and CDK4 protein levels (Figure 6F). Together, these results suggest that Y14 overexpression partially attenuates celastrol-induced NMD-associated changes and downstream p53/p21-related regulatory effects.

Celastrol modulates the ALYREF/FADS2/GPX4 pathway and lipid peroxidation-related redox changes in MDA-MB-231 cells

We also performed target validation for the other candidate target ALYREF in MDA-MB-231 cells treated with PROTAC_4. PROTAC_4 reduced ALYREF protein abundance, and this effect was attenuated by the proteasome inhibitor MG132, suggesting that PROTAC_4-mediated ALYREF reduction was associated with the ubiquitin-proteasome system (Figure 7A-B, Figure S5A-B). In the ligand competition assay, excess celastrol or the cIAP ligand B5 weakened PROTAC_4-induced ALYREF reduction, supporting the involvement of both the celastrol moiety and the E3 ligase ligand in this process (Figure 7C, Figure S5C). In addition, DARTS, CETSA and MST assays further supported the interaction between celastrol and ALYREF (Figure 7D-F, Figure S5D). Additionally, molecular docking was performed for ALYREF and celastrol, which suggested a possible binding mode involving residues PHE96, SER94, GLU154, and ARG155 (Figure S6). Collectively, these results suggest that ALYREF is a celastrol-associated target identified by the PROTAC-assisted target discovery strategy.

ALYREF is a specific mRNA m^5C-binding protein that can recognize m^5C-modified mRNA and promote its export from the nucleus. Previous studies have reported the transcriptomic profile of m^5C-modified mRNAs recognized by ALYREF.[32] By combining these transcriptomic data with the proteomics data in this study, both FADS1 and FADS2 were identified as potential downstream candidates related to ALYREF-associated regulation (Figure 3E).

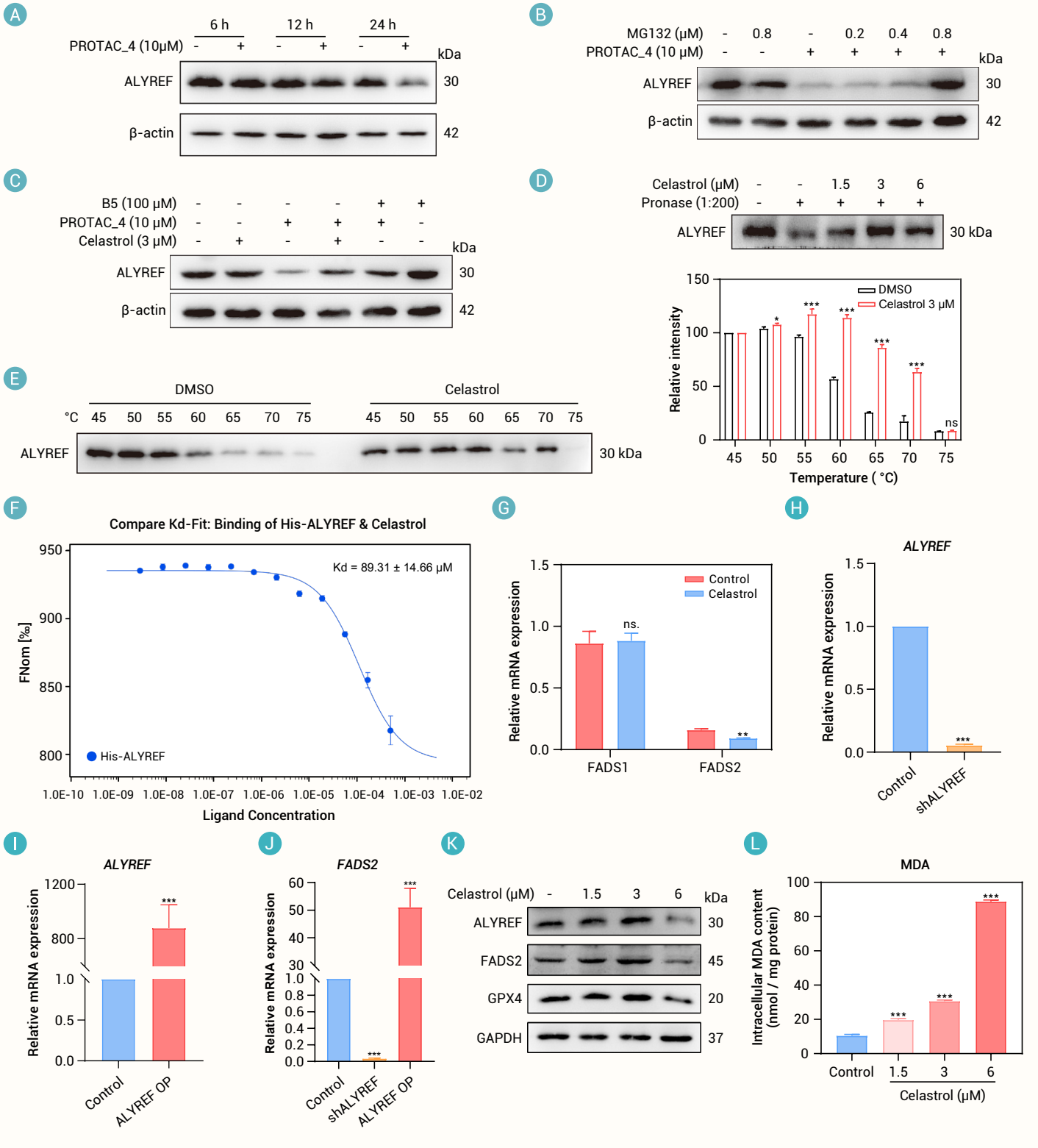


Figure 7. Celastrol modulates the ALYREF/FADS2/GPX4 pathway and lipid peroxidation-related redox changes in MDA-MB-231 cells (A) PROTAC_4 degrades the ALYREF protein in a time-dependent manner. (B) The reversal of PROTAC_4 degradation activity by MG132 in MDA-MB-231 cells. (C) The competitive inhibition of PROTAC_4 degradation activity by celastrol and B5 (cIAP ligand). (D) DARTS assay was performed to evaluate the effect of celastrol on ALYREF resistance to pronase digestion. (E) CETSA assay was performed to assess the effect of celastrol on ALYREF thermal stability. (F) MST assay was conducted to determine the binding affinity between celastrol and ALYREF. (G) Effect of celastrol treatment on mRNA levels of FADS1 and FADS2. (H-J) Changes in FADS2 mRNA abundance after ALYREF knockdown or overexpression. (K) Celastrol reduced GPX4 expression in MDA-MB-231 cells. (L) MDA levels were measured to evaluate lipid peroxidation-related changes. Data are presented as mean ± SEM. $^{**}p < 0.01$ vs. the DMSO group. $^{***}p < 0.001$ vs. the DMSO group. ns, no significance. The DMSO group served as the vehicle control, and the final DMSO concentration was 0.02% (v/v).

Therefore, we further investigated whether celastrol affected ALYREF-associated regulation of FADS1 and FADS2 expression. After celastrol treatment, only FADS2 mRNA abundance was reduced, whereas FADS1 remained unchanged (Figure 7G). ALYREF knockdown reduced FADS2 mRNA abundance, while ALYREF overexpression significantly increased FADS2 mRNA abundance (Figure 7H-J). Overall, these results suggest that FADS2 expres-

sion is associated with ALYREF status in MDA-MB-231 cells.

Subsequently, we examined whether celastrol-associated FADS2 down-regulation affected GPX4, a lipid peroxide-reducing enzyme involved in cellular redox homeostasis. Previous studies have shown that FADS1/2 regulate lipid metabolism in aggressive TNBC,[33] and FADS2 knockdown has been reported to reduce GPX4 expression.[34] We therefore examined the effects of celastrol on the ALYREF/FADS2/GPX4 axis. The results indicated that high concentrations of celastrol reduced GPX4 expression and increased MDA levels (Figure 7K-L, Figure S5E), indicating enhanced lipid peroxidation-related redox changes in MDA-MB-231 cells. Together, these findings suggest that celastrol-associated ALYREF modulation may affect FADS2 expression and downstream lipid redox homeostasis, as reflected by reduced GPX4 expression and increased MDA accumulation in MDA-MB-231 cells.

DISCUSSION

PROTACs have been widely applied to identify novel molecular targets. We develop it as an innovative approach for the target identification of natural products for the first time.[12] Ni et al. thereafter used PROTAC technology combined with IP-MS to identify the targets of celastrol in Jurkat cells, revealing potential targets such as NFκB, IKKβ, and PI3Kα.[35] However, the molecular targets and underlying mechanisms of celastrol exhibit variability across different cancer types. In this study, we utilized PROTAC technology to develop the understanding of "single drug with multiple targets", and found celastrol affecting multiple targets to produce therapeutic effects on TNBC cells.

In this study, we considered that different E3 ligases have distinct substrate recognition mechanisms, which can influence the spectrum of proteins degraded by PROTAC molecules. To explore more potential targets of celastrol, we designed and synthesized celastrol-PROTAC molecules with six different E3 ligase ligands. Based on the preliminary inhibitory activity screening results, we selected PROTAC_4, PROTAC_9 and PROTAC_18 as tool molecules for identifying the potential targets of celastrol. In the degradation proteomics data analysis, PROTAC_18 produced a relatively sparse degradome and was therefore less informative for convergence-based target discovery. In order to ensure the accuracy of the target information, we selected proteins that were degraded by both PROTAC_4 and PROTAC_9 molecules as candidate targets which were further verified by using various target validation techniques, including MST, CETSA, and DARTS. The molecular docking analysis further supported that celastrol binds to ALYREF, with hydrogen bonds formed at PHE96, SER94, GLU154, and ARG155 (Figure S6). Additionally, the full-length crystal structure of PYM1 is lacking, so molecular docking cannot be performed. These findings provide insights into the potential targets of celastrol and reinforce the utility of PROTAC technology in natural product target identification. However, the celastrol-based PROTACs generated in this study were mainly designed as target-identification tools for *in vitro* assays rather than as optimized therapeutic candidates for *in vivo* administration. Their potential *in vivo* application would require further structural optimization and pharmacokinetic evaluation, particularly considering their relatively high molecular weights and complex structures.

EJC plays a crucial role in post-transcriptional regulation by identifying mRNA containing PTCs, thereby triggering the NMD process. PYM1 interacts with the EJC, regulating its normal cycle. When PYM1 is inhibited or inactivated, the function of the EJC may be affected, leading to dysregulation of NMD-associated mRNA surveillance, which disrupts the balance of mRNA and results in cellular dysfunction. Our study identifies PYM1 as a celastrol-associated target. As PYM1 is a key regulator of EJC disassembly and NMD, celastrol may serve as a valuable chemical tool for studying these RNA surveillance mechanisms, thereby facilitating the discovery of novel modulators.

The identification of ALYREF further broadens the mechanistic understanding of celastrol beyond conventional protein signaling pathways. More importantly, PYM1 and ALYREF may be placed within a common framework of mRNA fate regulation rather than viewed as two completely independent targets. ALYREF functions as an mRNA export adaptor and m^5C reader, linking RNA modification to the nuclear export of selected mRNAs.[32] In contrast, PYM1 acts at a later stage of the mRNA life cycle by regulating EJC disassembly and recycling during translation-associated mRNP remodeling.[22-24] These two proteins are functionally connected through sequential steps of post-transcriptional gene regulation, including mRNA export, surveillance, translation-associated remodeling, and downstream gene expression control. From this perspective, celastrol may interfere with multiple RNA-regulatory checkpoints in MDA-MB-231 cells. Disruption of PYM1-associated EJC/NMD regulation may contribute to altered p53/p21 signaling and G1 phase cell cycle arrest, whereas interference with ALYREF-associated mRNA regulation may affect FADS2/GPX4-related lipid metabolic and redox homeostasis. Therefore, the simultaneous identification of PYM1 and ALYREF suggests that celastrol may exert antitumor effects in TNBC cells by coordinately perturbing mRNA fate regulation rather than acting through a single isolated signaling pathway.

CONCLUSION

Collectively, this study identifies candidate targets PYM1 and ALYREF for celastrol using PROTAC-based target identification technology. Furthermore, celastrol was found to engage PYM1 and ALYREF as candidate functional targets. Celastrol-associated perturbation of PYM1/EJC/NMD regulation may contribute to p53/p21 signaling activation and G1 phase cell cycle arrest, whereas modulation of the ALYREF/FADS2/GPX4 axis was associated with increased MDA accumulation and lipid peroxidation-related redox changes in MDA-MB-231 cells. These findings provide new insights into the mechanisms of celastrol against triple-negative breast cancer.

REFERENCES

1. Wang C., Dai S., Zhao X., et al. (2023). Celastrol as an emerging anticancer agent: Current status, challenges and therapeutic strategies. *Biomed. Pharmacother.* **163**:114882. DOI:10.1016/j.biopha.2023.114882
2. Tu Y., Dai G., Chen Y., et al. (2025). Emerging Target Discovery Strategies Drive the Decoding of Therapeutic Power of Natural Products and Further Drug Development: A Case Study of Celastrol. *Exploration.* **5**:e20240247. DOI:10.1002/EXP.20240247
3. Zhu Y., Meng Y., Zhang J., et al. (2024). Recent Trends in anti-tumor mechanisms and molecular targets of celastrol. *Int J Biol Sci.* **20**:5510–30. DOI:10.7150/ijbs.99592
4. Xu H., Zhao H., Ding C., et al. (2023). Celastrol suppresses colorectal cancer via covalent targeting peroxiredoxin 1. *Signal Transduct. Target. Ther.* **8**:51. DOI:10.1038/s41392-022-01231-4
5. Yang Y., Tse Y.S., Zhang Q., et al. (2024). Multiplexed Target Profiling with Integrated Chemical Genomics and Chemical Proteomics. *J. Med. Chem.* **67**:17542–50. DOI:10.1021/acs.jmedchem.4c01463
6. Yang F., Zhou H., Luo P., et al. (2024). Celastrol induces DNA damage and cell death in BCR-ABL T315I-mutant CML by targeting YY1 and HMCES. *Phytomedicine.* **134**:155937. DOI:10.1016/j.phymed.2024.155937
7. Liu D.D., Luo P., Gu L., et al. (2021). Celastrol exerts a neuroprotective effect by directly binding to HMGB1 protein in cerebral ischemia-reperfusion. *J. Neuroinflammation.* **18**:174. DOI:10.1186/s12974-021-02216-w
8. Luo P., Zhang Q., Shen S., et al. (2023). Mechanistic engineering of celastrol liposomes induces ferroptosis and apoptosis by directly targeting VDAC2 in hepatocellular carcinoma. *Asian J. Pharm. Sci.* **18**:100874. DOI:10.1016/j.ajps.2023.100874
9. Yuan Z., Wang J., Qu Q., et al. (2023). Celastrol Combats Methicillin-Resistant Staphylococcus aureus by Targeting Δ1 -Pyrroline-5-Carboxylate Dehydrogenase. *Adv Sci (Weinh).* **10**:e2302459. DOI:10.1002/advs.202302459
10. Zhu Y., Wan N., Shan X., et al. (2021). Celastrol targets adenylyl cyclase-associated protein 1 to reduce macrophages-mediated inflammation and ameliorates high fat diet-induced metabolic syndrome in mice. *Acta Pharm. Sin. B* **11**:1200–12. DOI:10.1016/j.apsb.2020.12.008
11. Wang L., Lin F., Liu J., et al. (2025). Revealing a new target: Celastrol alleviates pulmonary fibrosis by inhibiting PCAF. *Bioorg. Chem.* **163**:108722. DOI:10.1016/j.bioorg.2025.108722
12. Wu Y., Yang Y., Wang W., et al. (2022). PROTAC technology as a novel tool to identify the target of lathyrane diterpenoids. *Acta Pharm. Sin. B* **12**:4262–65. DOI:10.1016/j.apsb.2022.07.007
13. Bondeson D.P., Mares A., Smith I.E., et al. (2015). Catalytic *in vivo* protein knockdown by small-molecule PROTACs. *Nat. Chem. Biol.* **11**:611–7. DOI:10.1038/nchembio.1858
14. Li K. and Crews C.M. (2022). PROTACs: past, present and future. *Chem. Soc. Rev.* **51**(12):5214–36. DOI:10.1039/d2cs00193d
15. Liu Y., Liang J., Zhu R., et al. (2024). Application of PROTACs in Target Identification and Target Validation. *Acta Mater. Med.* **3**:72–87. DOI:10.15212/amm-2024-0010
16. Bray F., Laversanne M., Sung H., et al. (2024). Global cancer statistics 2022: GLOBOCAN estimates of incidence and mortality worldwide for 36 cancers in 185 countries. *CA Cancer J. Clin.* **74**:229–63. DOI:10.3322/caac.21834
17. Shrivastava S., Jeengar M.K., Reddy V.S., et al. (2015). Anticancer effect of celastrol on human triple negative breast cancer: possible involvement of oxidative stress,

mitochondrial dysfunction, apoptosis and PI3K/Akt pathways. *Exp. Mol. Pathol.* **98**:313–27. DOI:10.1016/j.yexmp.2015.03.031
18. Yan F., Wu Z., Li Z., et al. (2020). Celastrol inhibits migration and invasion of triple-negative breast cancer cells by suppressing Interleukin-6 via downregulating Nuclear Factor-κB (NF-κB). *Med. Sci. Monit.* **26**:e922814. DOI:10.12659/MSM.922814
19. Thompson A., Schäfer J., Kuhn K., et al. (2003). Tandem mass tags: a novel quantification strategy for comparative analysis of complex protein mixtures by MS/MS. *Anal. Chem.* **75**:1895–904. DOI:10.1021/ac0262560
20. McAlister G.C., Huttlin E.L., Haas W., et al. (2012). Increasing the multiplexing capacity of TMTs using reporter ion isotopologues with isobaric masses. *Anal. Chem.* **84**:7469–78. DOI:10.1021/ac301572t
21. Han X., Wei W. and Sun Y. (2022). PROTAC Degraders with Ligands Recruiting MDM2 E3 Ubiquitin Ligase: An Updated Perspective. *Acta Mater. Med.* **1**:244–59. DOI:10.15212/amm-2022-0010
22. Diem M.D., Chan C.C., Younis I., et al. (2007). PYM binds the cytoplasmic exon-junction complex and ribosomes to enhance translation of spliced mRNAs. *Nat. Struct. Mol. Biol.* **14**:1173–9. DOI:10.1038/nsmb1321
23. Gehring N.H., Lamprinaki S., Kulozik A.E., et al. (2009). Disassembly of exon junction complexes by PYM. *Cell.* **137**:536–48. DOI:10.1016/j.cell.2009.02.042
24. Brogna S., McLeod T. and Petric M. (2016). The Meaning of NMD: Translate or Perish. *Trends Genet.* **32**:395–407. DOI:10.1016/j.tig.2016.04.007
25. Carrard J. and Lejeune F. (2023). Nonsense-mediated mRNA decay, a simplified view of a complex mechanism. *BMB Rep.* **56**:625–32. DOI:10.5483/BMBRep.2023-0190
26. Thermann R., Neu-Yilik G., Deters A., et al. (1998). Binary specification of nonsense codons by splicing and cytoplasmic translation. *EMBO J.* **17**:3484–94. DOI:10.1093/emboj/17.12.3484
27. Gehring N.H., Neu-Yilik G., Schell T., et al. (2003). Y14 and hUpf3b form an NMD-activating complex. *Mol. Cell.* **11**:939–49. DOI:10.1016/s1097-2765(03)00142-4
28. Martin L., Grigoryan A., Wang D., et al. (2014). Identification and characterization of small molecules that inhibit nonsense-mediated RNA decay and suppress nonsense p53 mutations. *Cancer Res.* **74**:3104–13. DOI:10.1158/0008-5472.CAN-13-2235
29. Sureau A., Gattoni R., Dooghe Y., et al. (2001). SC35 autoregulates its expression by promoting splicing events that destabilize its mRNAs. *EMBO J.* **20**:1785–96. DOI:10.1093/emboj/20.7.1785
30. Mendell J.T., Sharifi N.A., Meyers J.L., et al. (2004). Nonsense surveillance regulates expression of diverse classes of mammalian transcripts and mutes genomic noise. *Nat. Genet.* **36**:1073–8. DOI:10.1038/ng1429
31. Gudikote J.P., Cascone T., Poteete A., et al. (2021). Inhibition of nonsense-mediated decay rescues p53β/γ isoform expression and activates the p53 pathway in MDM2-overexpressing and select p53-mutant cancers. *J. Biol. Chem.* **297**:101163. DOI:10.1016/j.jbc.2021.101163
32. Yang X., Yang Y., Sun B.F., et al. (2017). 5-methylcytosine promotes mRNA export - NSUN2 as the methyltransferase and ALYREF as an m^5C reader. *Cell Res.* **27**:606–25. DOI:10.1038/cr.2017.55
33. Lorito N., Subbiani A., Smiriglia A., et al. (2024). FADS1/2 control lipid metabolism and ferroptosis susceptibility in triple-negative breast cancer. *EMBO Mol. Med.* **16**:1533–59. DOI:10.1038/s44321-024-00090-6
34. Xuan Y., Wang H., Yung M.M., et al. (2022). SCD1/FADS2 fatty acid desaturases equipoise lipid metabolic activity and redox-driven ferroptosis in ascites-derived ovarian cancer cells. *Theranostics.* **12**:3534–52. DOI:10.7150/thno.70194
35. Ni Z., Shi Y., Liu Q., et al. (2024). Degradation-Based Protein Profiling: A Case Study of Celastrol. *Adv. Sci. (Weinh).* **11**:e2308186. DOI:10.1002/advs.202308186

FUNDING AND ACKNOWLEDGMENTS

This work was supported by the National Natural Science Foundation of China (NSFC) (No. U24A20784, 82473812), "Select the best candidates to lead key research projects" of Fujian University of Traditional Chinese Medicine (XJB2022008), Foundation of Fujian University of Traditional Chinese Medicine (X2023001-Talent), and Project of Frontier Technology Platform for Research Projects of Liaoning Provincial Department of Education in 2024 (LJ232410163056) for financial supports. And we acknowledged the support from National-Local Joint Engineering Research Center for Molecular Biotechnology of Fujian & Taiwan TCM, Fujian Key Laboratory of Chinese Materia Medica, Fujian University Key Laboratory for Research and Development of TCM Resources, at Fujian University of Traditional Chinese Medicine.

AUTHOR CONTRIBUTIONS

M.Z.: Conceptualization, methodology, validation, writing-original draft preparation. H.S.: Data curation, writing-original draft preparation, methodology. Y.L.: Validation, investigation. K.S.: Methodology, validation. H.C.: Methodology, validation. Y.Y.: Validation, visualization. D.S.: Writing-reviewing and editing. H.L.: Conceptualization, supervision, funding acquisition. L.C.: Project administration, funding acquisition. All authors contributed to the manuscript and approved the final version.

DECLARATION OF INTERESTS

The authors declare no competing interests.

ETHICAL STATEMENT AND PATIENT CONSENT

Not applicable.

DATA AND CODE AVAILABILITY

Data are available from the corresponding author upon reasonable request.

SUPPLEMENTAL INFORMATION

It can be found online at https://doi.org/10.59717/j.xinn-drugdisc.2026.100046.